ELSEVIER

Biophysical Chemistry 93 (2001) 103–127

Biophysical Chemistry

www.elsevier.com/locate/bpc

The diluted aqueous solvation of carbohydrates as inferred from molecular dynamics simulations and NMR spectroscopy

Søren B. Engelsen[a,*], Céline Monteiro[b], Catherine Hervé de Penhoat[b], Serge Pérez[b]

[a] *The Royal Veterinary and Agricultural University, Centre for Advanced food Studies, Rolighedsvej 30, DK-1958 Frederiksberg C, Denmark*

[b] *Centre de Recherches sur les Macromolécules Végétales, CNRS*[1], BP 53X, 38041 Grenoble cédex, France Affiliated with the Universit Joseph Fourier at Grenoble.

Received 19 March 2001; received in revised form 14 May 2001; accepted 15 May 2001

Abstract

The purpose of this paper is to review our understanding of the dilute hydration (aqueous solvation) behaviour of disaccharide compounds. To this end we discuss and scrutinise the results that have been obtained for the three model disaccharides: maltose, sucrose and trehalose from experimental NMR studies and from theoretical molecular dynamics studies in explicit aqueous solutions. The focus is on the description of molecular hydration features that will influence macroscopic entities such as diffusion and relaxation: residence times of hydration waters, hydration numbers and hydration densities. The principles of molecular dynamics simulation are briefly outlined while a detailed presentation is given of the key features that characterise hydration: the solvation of the glycosidic linkage, the radial hydration of the solute, the water density anisotropy around the solute, the residential behaviour of water molecules in the periphery of the solute, and rotational and translational diffusion coefficients. With respect to the use of NMR in characterising the structure and dynamics of the hydration, the hydrodynamic theory of rotational and translational diffusion of biomolecules as well as the use of pulse field gradient spin echo experiments are briefly presented. The NMR-defined rotational diffusion coefficients (D_r) and the experimentally determined translational diffusion (D_t) coefficients are reported for 4% (w/w) solutions of sucrose, trehalose and maltose. These results are compared with theoretical data obtained from molecular dynamics simulations of sucrose, trehalose and maltose under identical conditions (concentration, temperature, etc.). With our present level of knowledge we can propose

* Corresponding author. Tel.: +45-35-283205; fax: +45-35-283245.
E-mail address: se@kvl.dk (S.B. Engelsen).

PII: S0301-4622(01)00215-0

that although carbohydrates share a number of hydration characteristics, evidence is accumulating in support of the notion that it is not the amount or overall hydration but rather the detailed individual carbohydrate–water interaction that is likely to determine carbohydrate structure and functionality.

Keywords: Maltose; Sucrose; Trehalose; Hydration; Residence time; Molecular dynamics; NMR, Pulsed-field gradient spin-echo experiments; Translational diffusion measurements; Carbon longitudinal relaxation times

1. Introduction

Carbohydrates have a very high affinity to water, the predominant biological medium. They constitute a particularly interesting class of biological solutes, as the majority of their hydrogen bonding interactions with aqueous solvent occurs through their hydroxyl groups, which in their hydrogen-bonding scheme behave much like the water molecules themselves. In the case of sucrose the saturation solubility in water is 67.36% (w/w) at 25°C. It is therefore not surprising that carbohydrates affect the surrounding water structure and that, in return, the water affects the structure of the dissolved carbohydrate molecules. It is the nature of their interactions with water that is responsible (or decisive) for most carbohydrate biological functionalities including energy transport and storage, sweet taste induction, gel-phase formation, stabilisation and adherence and signal transmission, yet at the molecular level specific carbohydrate–water interactions remain largely to be elucidated. For this reason the next frontier in the understanding of carbohydrate structure and functionality will most likely be focused around their hydration.

Macroscopic thermodynamic studies of carbohydrate–water systems have a long and distinguished history due to their ability to probe some of the unique properties of hydrated carbohydrates. While such methods are excellent for describing the overall carbohydrate hydration, they do not provide evidence of the detailed hydration on the molecular level. Alone and especially when coupled with molecular simulation tools such as molecular dynamics with explicit water molecules, advanced NMR techniques provide an effective tool for investigating the detailed hydration of complex solutes such as carbohydrates. The first application of detailed dynamic perturbation methods such as high-resolution NMR to carbohydrate–water systems appeared approximately two decades ago in a study of the sucrose–water system [1]. Since then a large number of carbohydrate NMR studies have emerged. However, in the majority of such studies the focus has been more on the structure of the carbohydrate solute than on the detailed hydration. When focus is on the study of carbohydrate hydration, NMR and molecular dynamics techniques are generally considered strongly interdependent, but also complementary with respect to the timescales of the dynamic events under investigation. Condensed phase molecular dynamics simulations provide a means for studying dynamic events ranging approximately from the nanosecond down to the sub-femtosecond scale. This time range suffices for studying vibrational motions and most internal molecular transitions with the exception of torsional transitions around principal (backbone) conformational degrees of flexibility such as glycosidic linkages. Most important in these studies is that the time range covers the description of the dynamics of the hydration features. NMR, which is the most versatile and general experimental technique available for studying molecular dynamics, will under normal conditions use perturbation times in the micro and millisecond ranges and thereby 'only' provide time averaged dynamic information about sub-microsecond events.

In order to fully understand results from modern experimental perturbation methods it is imperative to have a reliable theoretical model of solvation dynamics and it would appear as if

molecular dynamics provides the most promising technique for this purpose. Molecular dynamics studies of carbohydrates in aqueous solution were pioneered a little more than one decade ago by Grigera with a study on mannitol and sorbitol [2], by Koehler et al. with a study on α-cyclodextrin [3], by Brady with a simulation of glucose [4] and by van Eijck and Kroon with simulations of ribose and deoxyribose [5]. These investigations came approximately one decade later than the first simulation of a dipeptide in water by Rossky and Karplus [6], a milestone in the field of simulations of dissolved molecules in water. While the elucidation of the hydration of the monosaccharides is essential for the understanding of basic carbohydrate compatibility with the water structure, the understanding of the hydration of the glycosidic linkage will clarify conformational preferences of the overall carbohydrate structure in water. Studies on model disaccharides such as maltose [7,8], Manα(1 → 2)Manα [9], Manα(1 → 6)Manα [10] cellobioside [11], sucrose [12–14], neocarrabiose [15] and α,α-trehalose [16–18] have all clearly demonstrated that the presence of water has a significant impact on the principal conformational parameter that governs the overall molecular shape, namely the glycosidic linkage orientation.

Among the limited number of molecular dynamics investigations of disaccharides only two have been performed using the same protocols and conditions (force field, parametrisation, model of water) over a sufficiently long period of time; these are sucrose and trehalose. This work aims at reviewing key hydration features in a comparative hydration study of sucrose and trehalose and in some cases with reference to maltose. Moreover, this study reports new experimental NMR evidence of the influence of carbohydrates on the water structure. When examining the hydration of sucrose and trehalose in detail it is perhaps surprisingly found that their hydration pattern is entirely different, supporting our present hypothesis that carbohydrate–water interactions are highly specific and in principle designed for different tasks such as restricted diffusion of water, restricted diffusion of carbohydrate, structural motif lock and water channel/pump.

2. Methods

2.1. The carbohydrate molecules and nomenclature

In this work we will discuss the hydrations of the three disaccharides sucrose, maltose and trehalose.

Table sugar, or sucrose β-D-fructofuranosyl-(2 → 1)-α-D-glucopyranoside; Fig. 1a), is a non-reducing disaccharide present in all photosynthetic plants where it functions as a transport substance during starch translocation and in some plants as an energy supply. Sucrose contains two neighbouring anomeric centres, C-1g and C-2f, and exhibits an overlapping exo-anomeric effect due to the sequence C-5g-O-5g-C-1g-O-1g-C-2f-O-5f-C-5f. Sucrose is the most abundant disaccharide in nature, but despite the fact that sucrose has been subjected to intensive modern research for approximately 100 years, we are only beginning to understand the unique properties of this molecule, including structure in aqueous environment, supersaturation behaviour and sweet taste induction.

Mushroom sugar, or α,α-trehalose (α-D-glucopyranosyl-(1 → 1)-α-D-glucopyranoside; Fig. 1b), is the only naturally occurring disaccharide out of three isomeric trehalose forms (αα, αβ and ββ). In the (C_2) symmetric α,α-trehalose, two α-D-glycosyl units are linked by a glycosidic linkage between their two anomeric carbon atoms, abbreviated to C-1 and C-1′, exhibiting the so-called double anomeric effect throughout the sequence: C-5-O-5-C-1-O-1-C-2′-O-5′-C-5′. Trehalose has a hydration characteristic, which displays extremely interesting features including the ability to protect and reversibly reconstitute proteins and biomembranes from dehydration, a glass-transition anomaly, the ability to retain and preserve volatile flavours and aromas in dried foodstuffs, etc. Trehalose is produced by many cryptobionts in both the plant (spores of certain fungi and a few varieties of plant seeds) and the animal kingdoms (desert insects, brine shrimp embryo, baker's yeast) and survival of anhydrobiosis and cryptobiosis by many of these organisms was found in the early 1980s to be correlated with the presence of trehalose [19,20]. Since then a large number of

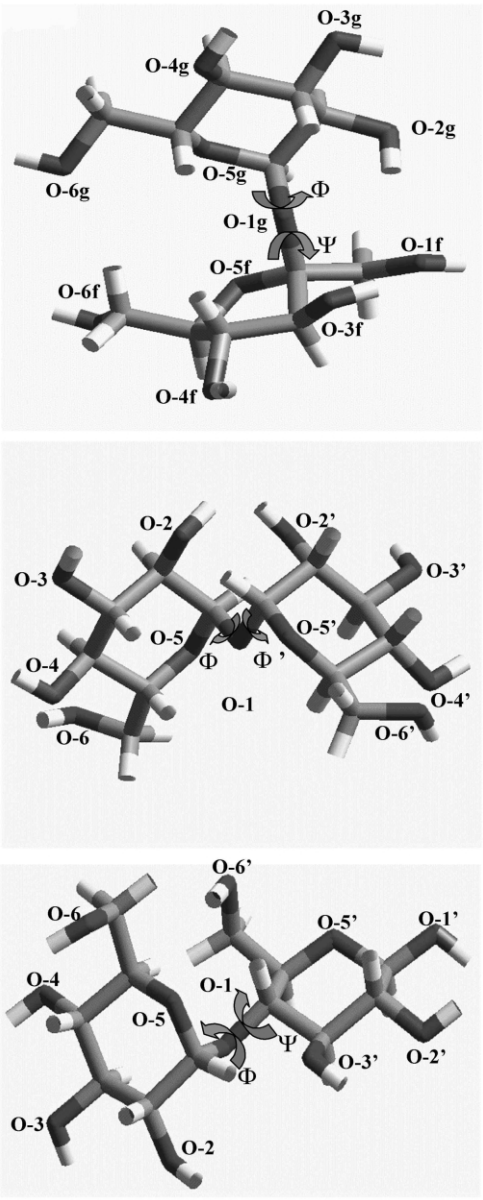

Fig. 1. Labelling and heavy atom representations of sucrose, trehalose and maltose with indications of glycosidic dihedrals Φ and Ψ. (a) Sucrose: Φ = O-5g–C-1g–O-1g–C-2f and Ψ = C-1g–O-1g–C-2f–O-5f. (b) Trehalose: Φ = O-5–C-1–O-1–C-1′ and Ψ = C-1–O-1–C-1–O-5′. (c) Maltose: Φ = O-5–C-1–O-1–C-4′ and Ψ = C-1–O-1–C-4′–C-5′.

studies have been performed to disclose the mechanisms behind trehalose functionality, with research mainly driven by the potential interests in medical protein stability.

α-Maltose (α-D-glucopyranosyl-(1 → 4)-α-D-glucopyranose; Fig. 1c), like sucrose, is basically an energy storage molecule and is most abundant as the building element of the starch components amylose and amylopectin. Due to the extreme importance of starch in areas spanning from bread baking to material science, the structure and hydration of maltose has received much attention in the literature.

Conformational flexibility around the glycosidic linkage bonds is described by the two torsional angles: Φ and Ψ (Fig. 1). The conformations of the two hydroxymethyl groups are described by the torsional angles: ω = O-5–C-5–C-6–O-6, ω′ = O-5′–C-5′–C-6′–O-6′ and for the second hydroxymethyl group on the fructofuranose ring in sucrose: χ^f = O-5′-C-2′-C-1′-O-1′. The three staggered orientations of the primary hydroxyl groups are also referred to as either *gauche–gauche* (GG), *gauche–trans* (GT) or *trans–gauche* (TG), depending on whether the values of the above torsion angles are closest to −60°, 60° or 180°, respectively. The sign of the torsion angles is defined in agreement with the IUPAC Commission of Biochemical Nomenclature [21].

A prerequisite to understanding the biochemical functions is a detailed description of the constitution, the configuration and the conformation of solutes in the solid state. Two of the three model disaccharides, sucrose [22] and β-maltose [23], have been investigated by single crystal neutron diffraction. α,α-Trehalose has been studied by single crystal X-ray diffraction in its dihydrate form [24,25] as well as in its low temperature anhydrous form [26]. In addition, the α-anomer of maltose has been studied with single crystal X-ray diffraction [27].

3. Molecular dynamics

3.1. Background

In addition to rotational and vibrational motions, atoms also exhibit *thermal motions*. The

most distinguished task of molecular dynamics is to analyse thermal motions of molecules driven by intramolecular as well as by intermolecular collisions. Thermal motion is not oscillatory, which implies that in principle we have to calculate the equations of motion over an indefinite period of time in order to sample all possible geometries. However, in practice it is possible to explore a potential-energy-well in a finite time period.

The molecular dynamics method concept involves calculating the displacement co-ordinates in time (a trajectory) of a molecular system at a given temperature. Finding positions and velocities of a set of particles as a function of time is done classically by integrating Newton's equations of motion in time. Molecular dynamics simulations are usually carried out as a micro-canonical (constant-*NVE*) or canonical (constant-*NVT*) ensemble, thus all other thermodynamic quantities must be determined by ensemble averaging. In a classical system, Newton's equations of motion conserve energy and thus provide a suitable scheme for calculating a micro-canonical ensemble. However, canonical ensemble can readily be performed by coupling the molecular system to a constant-temperature bath, which rescales the atomic velocities according to the desired temperature. In a similar manner, constant pressure simulations can be performed by scaling through coupling to a constant-pressure piston, as the pressure can be calculated from the virial theorem. The first simulations on hard-sphere liquids were performed by Alder and Wainwright in the late 1950s [28] where the particles were only allowed to move with constant velocity between perfect elastic collisions. It was only when Stillinger and Rahman [29] published their classic study of liquid water in 1974 that molecular dynamics became an established theoretical method for studying thermodynamic properties and molecular motions. While many of the early molecular dynamics studies were made in the liquid field, interest soon focused on modelling motions in biomolecules. Modelling biomolecules differs from the liquid simulations in that, until recently, it has only involved one molecule's trajectory, and in that the system (particle) has a large number of (internal) covalent bonds. In the field of biomolecules, the study of the small protein Bovine Pancreatic Trypsin Inhibitor (BPTI, 454 extended atoms) has served as a model [30–32]. Using a step size in the femtosecond regime has some very important implications when studying atomic motions, as the calculation of a single trajectory in one microsecond involves 1 billion evaluations of the potential energy functions using the Verlet algorithm. For this reason one cannot overestimate the importance of optimising the function evaluation. Combined atomic motions such as side chain motions can open pathways for ligands to enter, exit and close active sites, all very important motions determining biological activities and within the range of molecular dynamics (time scale of 10^{-15} s to 10^{-1} s — for unconstrained condensed-phase simulations as discussed in this paper the upper limit is approx. 10^{-6} s). As such, the molecular dynamics method is unique, in that it offers the possibility to verify theories about many important biological activities.

3.2. Molecular dynamics and carbohydrates

A prerequisite to carry out realistic molecular dynamics simulations is to have reasonable force fields for both the carbohydrate solute and for water at hand. With respect to the carbohydrate solute, a number of modified force fields are available for most established modelling packages [33]. When it comes to appropriate force fields for representing water, the choice is limited, but also more reliable. Basically, there is the choice between three-site models and five-site models including the lone-pair positions, however, for simulations of carbohydrate–water interactions the three-site water potentials have mainly been used. In general, the performance of the three-site water potentials offers a good compromise between performance and accuracy [34], and the choice of water model should therefore be guided by the interplay between the solute potentials and the water potentials. In this work we will focus on two molecular dynamics simulations of sucrose and trehalose, respectively, which are unique in that they have been recorded in the same carbohydrate force field [35] using the same water

potential, TIP3P [34], at almost the same concentration of approximately 4% (w/w).

4. Carbohydrate solvation

When analysing molecular dynamics simulations of, e.g. carbohydrates in solution, two pressing questions seek to be answered: (i) *did any intra-molecular hydrogen bonds persist in aqueous solution?* and (ii) *did the solute structure change significantly from its solid state structure?* Obviously, the two questions are interrelated but the first one is easier to answer. The classical technique for solving this question is to record hydrogen bond time series of the (realistic) C–O–H…O–C distances.

4.1. Intra-molecular hydrogen bonds

In the case of sucrose, X-ray studies indicate an almost spherical molecule stabilised by two intramolecular hydrogen bonds: O-1f–H...O-2 and O-6f–H...O-5g. Of all possible intramolecular hydrogen bonds the distance time series between O-1f–H and O-2g displayed in Fig. 2 was the most populated and yet below 5% of the entire trajectory time of the molecular dynamic simulation [14]. Apparently the intramolecular hydrogen bonds are supplanted by hydrogen bonds to the more mobile water molecules due to entropic considerations even when intramolecular donor-acceptor geometry is favourable. In the case of trehalose, intramolecular hydrogen bonds were not observed in the solid state and indeed no intramolecular hydrogen bonds were observed in the molecular dynamics trajectory. In the case of maltose, the situation concerning the crystallographic O-2…H–O-3′ hydrogen bond is more problematic, as one study has indicated that it prevails [7], whereas another study has shown that it is only weakly populated [8]. These disaccharide molecular dynamics studies collectively suggest that intramolecular hydrogen bonds in aqueous solution must represent sterically restricted situations where the increased entropy from water interactions cannot come into play. Unfortunately, NMR has not been very helpful in unravelling these points about intramolecular hydrogen bonds, mainly because the hydroxyl protons undergo chemical exchange and therefore are invisible in most NMR experiments. However, it is possible to measure hydroxyl proton signals in super-cooled solutions, but the realism of such experiments is difficult to judge. In the case of sucrose, the existence of ‘a weak and at least transiently existing’ O-2g...O-1f intramolecular hydrogen bond was reported from ROESY (two-dimensional rotating-frame exchange NMR spectroscopy) experiments in super-cooled solutions [36].

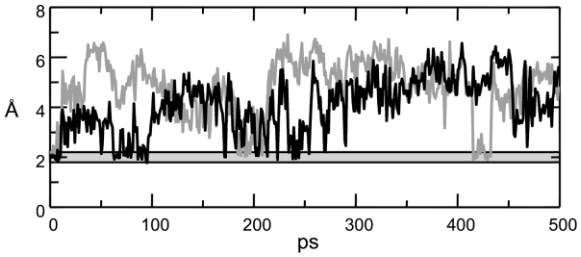

Fig. 2. Time series from the sucrose trajectory monitoring the O-2g…HO-1f hydrogen-bonding distance as derived from molecular dynamic simulations.

4.2. Solvation of the glycosidic linkage

Only limited response can be given to the second pressing question concerning any overall change in solute conformation. Indeed, when disaccharides and oligosaccharides have been studied the focus has been on the major conformational feature namely the glycosidic linkage. Changes in this conformational parameter are bound to give rise to profound changes in the experimental data when, e.g. comparing solid-state information with aqueous solution. Analogous to the hydrogen bond distance time series displayed in Fig. 2, it is common practice to calculate time series of the two main glycosidic parameters Φ and Ψ [16], but in this case they are more illustratively added as a scatter plot on top of an energy (adiabatic) map [17]. Alternatively, the information can be displayed as a population density map (Φ and Ψ

for each trajectory point is calculated and added to the relevant bin) as a function of the two main glycosidic parameters Φ and Ψ. This plot indicates the probability of finding the molecule with a glycosidic linkage in a given geometry. In the case of sucrose, the population density is depicted in Fig. 3 along with the adiabatic energy map computed in vacuum. From the figure it is evident that the preferred glycosidic conformation of sucrose is maintained in vacuum, in solid state and in aqueous solution. As early NMR evidence strongly suggested that sucrose remained in this potential-energy-well, sucrose was labelled a 'conformationally' rigid molecule and this conformation was thought to be the bio-active conformation. However, molecular dynamics simulations suggest that the mean potential acting on the solute is softened upon aqueous solvation due to the absence of prevailing intramolecular hydrogen bonds. This is demonstrated by an increase in root mean square fluctuations of the important glycosidic dihedrals and by the fact that the crystal conformation of the sucrose moiety in raffinose (additional $\alpha(1 \rightarrow 6)$ linked D-galactose residue) also appears in a highly populated area in contrast to the in vacuo adiabatic map where the crystal conformation was placed in a saddle-point region. In this case the aqueous solvation evidently induces the conformational flexibility (shift) necessary for the creation of the crystal nucleus that is able to propagate. In the case of trehalose, Fig. 4, the global energy minimum in vacuo (arrow) is shown to be far from the conformation found in crystalline state and by molecular dynamics in aqueous solvation. From the figure we observe that the presence of water is modifying the mean potential acting on the trehalose solute and that the population contours have become almost ellipsoid in contrast to the 'mouth-shaped' well on the adiabatic map (Fig. 4, left). Again it would appear that we observe a weak softening of the potential and a slight but significant asymmetry in the dihedral conformation of the trehalose solute induced by the presence of water.

While NMR was not able to settle, in a convincing manner, the intramolecular hydrogen bond issue, it can nevertheless help to assess the

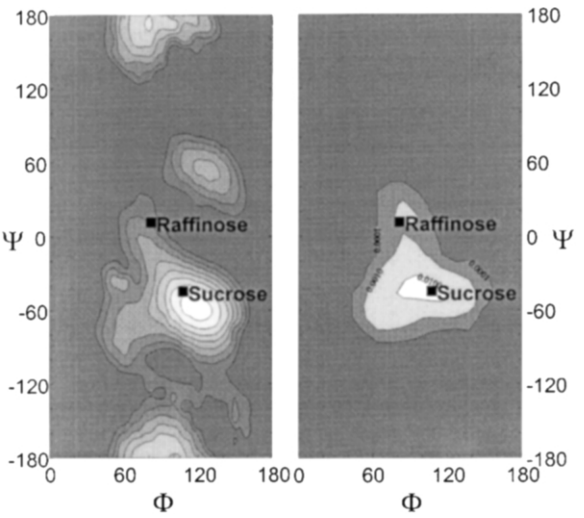

Fig. 3. (a) The in vacuo potential energy surface in the Φ,Ψ-space of sucrose recorded in a modified CHARMM force field (kcal/mol scale) and (b) the population density recorded from a molecular dynamics trajectory in aqueous solution (exponential population scale). The labels correspond to the positions of crystal structures of sucrose, raffinose. Adapted from Engelsen et al. [14].

motional averaged glycosidic geometry. Through heteronuclear coupling constants across the glycosidic linkage and an appropriate parametrisation of the Karplus equation [37] we can obtain a robust mutual connection between the ensemble averaged molecular dynamics simulation and the NMR experiment. In the sucrose case, the ensemble-averaged glycosidic heteronuclear coupling constant $^3J_{\text{H-1,C-2'}}$ for sucrose was calculated to 4.1 Hz from the solution trajectory, in excellent agreement with the experimentally measured 4.2 Hz value. The good agreement contrasts with the population-averaged value of 5.4 Hz derived from the in vacuo simulations, being dominated by the influence of the O-2g...H–O-1f internal hydrogen bond [14]. In the case of trehalose, the heteronuclear coupling over the dihedral linkage was calculated to 1.5 Hz in vacuo and to 2.2 Hz in the molecular dynamics simulation, which has to be compared with experimental values in the range of 2.5–3.3 Hz [38,39]. These results strongly suggest that water has to be taken into account in order to reliably model carbohydrate structure in aqueous solutions.

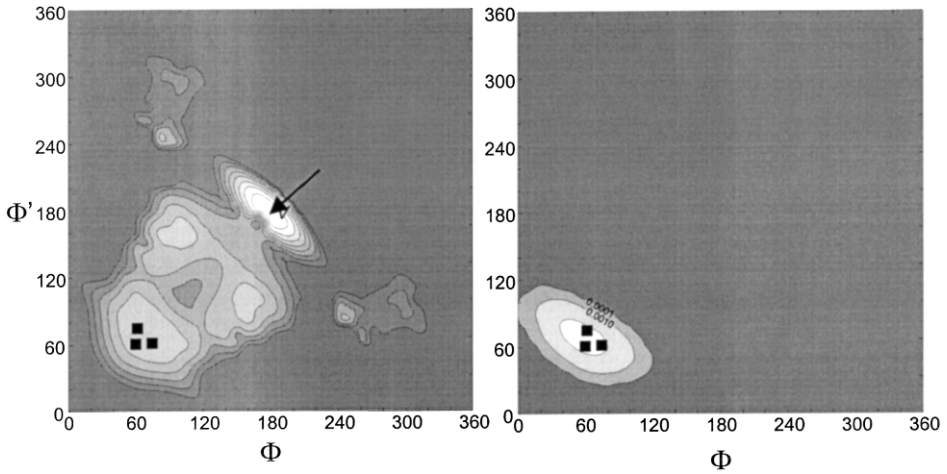

Fig. 4. (a) The in vacuo potential energy surface in Φ,Ψ-space of trehalose recorded in a modified CHARMM force field (kcal/mol scale) and (b) the population density recorded from a 1-ns molecular dynamics trajectory in aqueous solution (exponential population scale). The labels correspond to the positions of crystal structures of the dihydrate (asymmetric, hence two points) and the anhydrous structures. Adapted from Engelsen and Pérez [18].

5. Carbohydrate–water interactions

5.1. Radial hydration

Molecular dynamics simulations of solutes in water provide a unique possibility for detailed examination of water–solute interactions. However, when such simulations are performed, the question arises: *How does one characterise water solvating a complex solute?* [40]. The large number of water molecules, the complexity of the solute and the high degree of mobility in such simulations require a statistical approach to describe the hydration. The statistical approach most commonly employed to examine water–water and water–solute interactions is radial pair distribution function, *rdf*, that calculates the probability of finding a pair of atoms a distance *r* apart, relative to the probability expected for a random distribution at the same density. Within a crystalline arrangement the *rdf* will consist of spikes reflecting the structure of the lattice structure, while the *rdf* for an ideal gas would be a horizontal line reflecting an even distribution. For pure liquid systems such as water the *rdf* have an experimental background, as the oxygen–oxygen *rdf* can be measured from X-ray scattering experiments, assuming that the X-ray intensities are dominated by spherical scattering centred at the oxygens [29]. In more complex aqueous simulations, *rdf* of specific solute nuclei and the oxygen nuclei in water have been used in the literature to describe the large differences in the first and second hydration shells of different types of solute atoms. This is particularly suited for carbon in methyl and methylene groups, which display a typical hydrophobic behaviour, and around oxygen in hydroxyl groups, which display a typical hydrophilic behaviour [41]. Fig. 5 displays typical *rdf* for the atoms at the secondary hydroxyl group OH-2g (sucrose) with respect to the water oxygen atoms (Ow). The first sphere of nearest neighbours is indicated by a peak in *rdf* and limited by a minimum in *rdf*; it is referred to as the *first hydration shell*. This shell-type liquid structure is induced by the carbohydrate solute and it decreases in order with the distance. This is due to optimal average arrangements of the water hydrogen bonds. The first hydration shell around the HO-2 hydrogen (hydrogen bond donor) has a peak at approx. 1.9 Å with a density of 1.5 times the bulk density (Fig. 5). The first hydration shell is limited by the minimum density of less than 0.5 times the bulk density at approximately 2.2 Å.

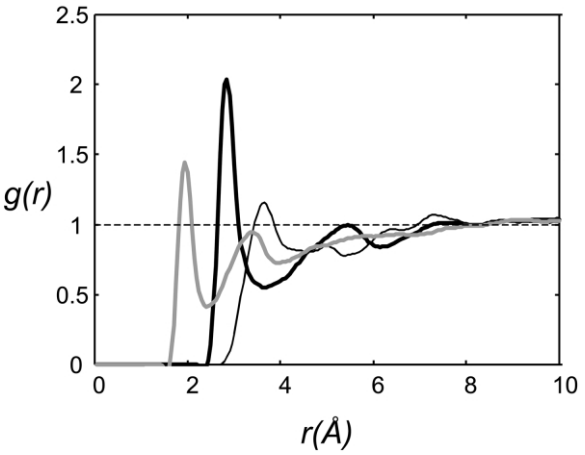

Fig. 5. Radial pair distribution functions calculated from a molecular dynamics trajectory of sucrose: (a) HO-2g…Ow (light grey), (b) O-2g…Ow (black) and (c) C-2g…Ow (dark grey).

The hydration shell around the O-2 oxygen (donor and acceptor) has a peak at 2.8 Å with a density of 2.2 and is limited at approximately 3.5 Å by the minimum density of approximately 0.5. While both the hydrogen and the oxygen pair distributions exhibit a pronounced secondary hydration shell, the long-range order in the hydration around the less exposed C-2 is more complex, but it still possesses a clear first hydration shell. In carbohydrate simulations attempts have been made to use radial pair distribution functions to scrutinise the detailed hydration pattern around solute atoms [4,5,13]. However, due to complicated dynamic and steric effects, the lack of ubiquitous discriminating functional forms of similar types of $g(r_{Os},r_{Ow})$ introduced below and lack of experimental evidence, the results of such efforts are generally not convincing.

This information may in principle be improved by using orientational pair distribution functions [6] which are applied to characterise the orientational preferences of local (first hydration shell) water molecules around solute atoms (X…H-Ow), but can also be used to examine the orientational preferences of water density with respect to a given solute vector, e.g. C-O…Ow [13]. However, much like in the case of the radial pair distributions, orientational pair distributions rarely bring new insight, when applied to carbohydrates due to their complex nature. While the *rdf* is generally not very informative, it introduces a very useful concept, namely, *the first hydration shell*. The close proximity of the eight hydroxylic and three acetalic oxygens leads to many shared water molecules among different solute oxygens, and obvious questions arise, such as: w*hat is the total number of water molecules inside the first hydration shell of all solute oxygens?* and *are shared water molecules a dominant feature of the solute structure?*

The hydration number is a fuzzy parameter to describe hydration of carbohydrates, as is reflected by the range of the experimental determinations of this parameter for sucrose: from $h = 21$ (near infrared spectroscopy) to $h = 1.8$ (NMR), depending on the experimental technique applied [42]. Molecular dynamics simulations provide a simple definition of this hydration parameter which can easily be calculated and compared to the experimental disorder: from the trajectory the number of water molecules in the first hydration shell (less than 3.5 Å) associated with the solute oxygens is counted in each phase point and an average is obtained. Much in line with the results derived from the radial pair distribution functions the calculated hydration numbers for sucrose and trehalose are identical: $h = 27.5$ first hydration shell water molecules per solute molecule. If instead of using the entire first hydration shell, the hydration criterion is restricted only to include distances less than 2.8 Å where the hydration of hydroxylic oxygens reaches maximum density, a value of $h = 7.8$ is obtained. However, the simulation is not able to contrast the hydration numbers of sucrose and trehalose. Two experimental studies include both the hydration number for sucrose ($h = 6.8$ [43]; $h = 6.33$ [44]) and trehalose ($h = 8.0$ [43]; $h = 7.95$ [44]), respectively.

5.2. Water density anisotropy

To quantify and visualise shared water densities amongst solute oxygens it is possible to calculate and contour three-dimensional water densities in a fixed frame defined by the solute [40,45].

However, this approach has two major disadvantages, namely, the difficulties in visualising the densities in three dimensions, and the fact that it is only useful for rigid molecules or rigid molecular segments. The hydration around monosaccharides and other relatively rigid molecules can be very well described by static water densities or radial pair distributions with only one reference point. However, the presence of the glycosidic linkage in oligosaccharides introduces such a high degree of flexibility that another approach for describing the hydration pattern is desirable. The normalised two-dimensional radial pair distribution function [46] is one such tool for analysing the solute surroundings for localised water densities around highly flexible molecules such as bridging water molecules between two sugar rings in carbohydrates.

The two-dimensional radial pair distribution function $g(r_1, r_2)$ calculates the probability of finding an atom (e.g. water oxygen) at a distance r_1 and r_2 from two selected solute atoms, relative to the probability expected for arandom distribution [46]:

$$g(r_1,r_2) = \frac{N(r_1,r_2)}{\rho_w \times V_{\text{intersect}}(r_1,r_2)} \quad (1)$$

The calculation of two-dimensional radial pair distribution functions is analogous to one-dimensional radial pair distribution, except that the histogram is now two-dimensional, referring to two reference points (nuclei) instead of one, and the normalisation is more complicated. The two-dimensional radial pair distribution functions have to be normalised using the intersection volume of the two sphere shells, $V_{\text{intersect}}$ (Fig. 6) in order to be relative to bulk density (equal to 1).

Fig. 7 (upper) displays the contour plot of an intra-ring normalised two-dimensional *rdf* of water in which the solute atoms O-2g and O-3g of sucrose are the reference sites. Such plots share some features with the potential energy plot commonly employed to study simple reaction collisions, except that the two-dimensional *rdf* usually has a minimum energy (maximum probability) with build-up of shared water density and not a transition. If scatter trajectories of water molecules are superimposed, it would be possible to study successful and unsuccessful encounters (attack) with the specified water pocket. The maximum shared water density of 5.6 times the bulk density (1.0) is found in the lower left corner (2.8 Å, 2.8 Å) and is a result of an advantageous position of the water in the centre of the first hydration shell of the two solute oxygen's. This shared maximum density is stronger than the average one-dimensional *rdf* peak density (approx. 2.2) of the first hydration shell, indicating a substantial anisotropy of the latter. At longer distances from the two solute oxygens we find less structured water (in the given reference) and observe that the shared water density approaches 1.0, corresponding to the bulk density. The steep decline of shared water densities to zero at approximately 6 Å is simply explained by the fact that it is an impossible situation, as the two sphere shells do not intersect (see Fig. 6). In the trajectory the average O-2…O-3 distance was 2.88 Å, ranging from 2.55 to 3.27 Å, allowing also for a direct but geometrically restricted hydrogen bond. When applying two-dimensional *rdf* to hydroxylic oxygens placed on opposite sucrosyl rings, we found two very strong shared water densities. Fig. 7 (lower) displays the two-dimensional *rdf* between O-2 and O-3′ from which we observe a very sharp and strong shared water density with a peak density of approx. 4.6 times bulk water density. In the case of the O-2…O-3′ distance, the

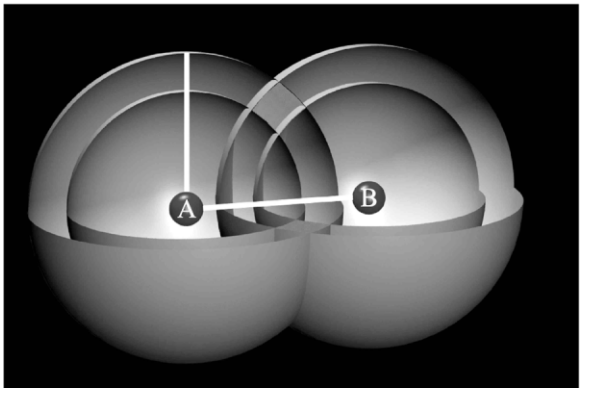

Fig. 6. Illustration of the intersection volume formed by the two sphere shells surrounding the two solute oxygen atoms: A and B.

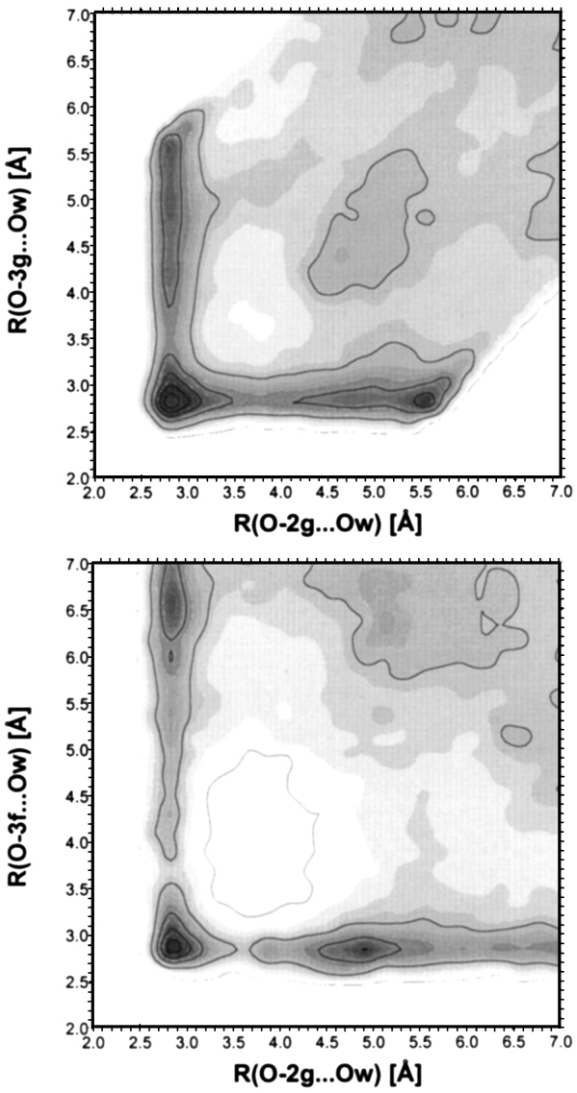

Fig. 7. Two-dimensional radial pair distribution functions for sucrose. Upper: neighbouring intra-ring water density O-2g…Ow…O-3g. Lower: inter-ring bridging water density between O-2g…Ow…O-3f. Adapted from Andersson and Engelsen [46].

trajectory average was 5.08 Å, ranging from 4.07 to 6.10 Å, indicating a rather flexible situation for the two reference atoms across the glycosidic linkage and accordingly, the bridging water situation was only found to populate 40% of the trajectory time.

In most cases only the two-dimensional *rdf* peak density will be of interest [47] and Fig. 8 displays all possible peak two-dimensional *rdf* densities around sucrose. The fact that these peak densities do not exactly correspond to the peak densities given above is due to the relatively sparse statistical sampling as well as to very sharp density build-ups which have been averaged (smoothed) by too coarse a grid size of 0.2×0.2 Å during contouring. Most interestingly we observe an extremely strong and sharp shared water density with a peak maximum of approx. 9 times the bulk density between O-2g and O-1f. This is an extreme situation, being more populated than a shared water between two neighbouring pyranose hydroxyl groups (Fig. 7). This is thus far the best example of a localised or 'pocket' water molecule that has been detected in a condensed phase molecular dynamics simulation of small carbohydrates. In the case of trehalose the maximum two-dimensional *rdf* density of an inter-ring shared water was calculated for O2…O4′ to be 2.4. This is a rather low value when compared to the maximum shared inter-ring water density of sucrose, and comparable in level to the maximum water density in the one-dimensional *rdf*, i.e. isotropically hydrated. Rather than displaying unique hydration features, trehalose solvation displays a remarkable resemblance to the crystalline-state hydration in the dihydrate polymorph [18]. Sucrose solvation, however, displays unique features and, although the representation of sucrose in Fig. 8 is schematic, it appears that the hydration needs for the sucrose structure are primarily optimised to satisfy the hydration along one side, defined by the oxygens O-4g…O-3g…O-2g…O-1g…O-1f…O3f. On the other side of the molecule, the shared water densities are either weak, comparable with the expected densities in a first hydration shell (2.2), or absent, as in the central region around the ring oxygens. To investigate the inter-ring bridging waters in more detail, the occurrence for each water molecule of staying in either the shared first hydration shell between O-2g and O-1f or between O-2g and O-3f (less than 3.5 Å) is plotted as a function of the trajectory frame (Fig. 9). From the figure we observe that the encounters last up to approximately 50 picoseconds (ps) and that there

appears to be significant co-operative effects between the two sites. However, due to the proximity of the two sites, it is perhaps not surprising to see significant co-operative effects, especially during the longer encounters. In Fig. 10 the trajectory of the water molecule [47] (number 288), which stays from approximately 130 to 200 ps in the inter-ring hydration site, is superimposed on a van der Waals surface of sucrose. The figure shows how the water molecule explores the oblong cavity defined by O-2g on one side and O-1f and O-3f on the other side for almost 80 ps. It helps to illustrate the concerted action of this hydration site that starts by a 'capture' via the O-3f group. Given the high probability of finding a water molecule in this cavity and the very good agreement with experimental descriptors provided by the molecular dynamics simulation [13,14], it is very tempting to propose that this hydration characteristic is of prime importance to the sucrose functionalities. That this water cavity in sucrose hydration is an important phenomenon is underlined by a more recent crystal structure determination of a lentil lectin [48] in which two partially hydrated sucrose molecules were buried in the binding site. Both of these sucrose structures were observed to be hydrated with an inter-ring bridging water molecule (oxygen) between O-2g and O-3f. One of the two partially hydrated sucrose molecules is displayed in Fig. 11 along with the water molecules in close proximity. The hydration waters display a striking but possibly random resemblance to the water trajectory displayed in Fig. 10.

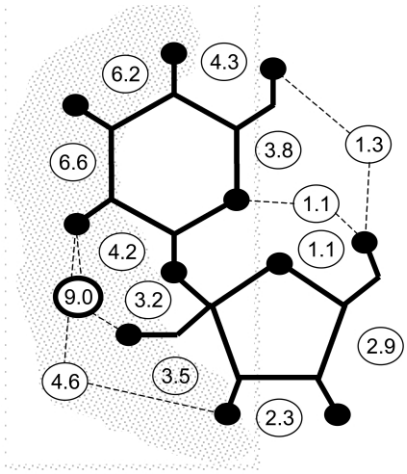

Fig. 8. Maximum shared water densities amongst sucrose oxygen atoms as calculated by normalised two-dimensional pair distribution functions at Os…Ow distances equal to 2.8 Å. Densities crossing the glycosidic linkage are indicated with dotted lines. Adapted from Engelsen [47].

5.3. Residential behaviour of water molecules

Before discussing how NMR can detect such complex hydration phenomena as described above, it is of prime importance to establish the time scales of such carbohydrate–water interactions. As also indicated by Fig. 10 a dynamic exchange of water molecules in the first hydration shell occurs and obviously the average time spent strongly associated with the solute is a hydration parameter of great interest. We have previously reported longer [13] residence times of water molecules around sucrose, as derived from an analysis that only took into account one water molecule at a time (frame). The residence time distributions as a function of time was expected to afford a more thorough description of the residence characteristics. An example of one such distribution is displayed in Fig. 11, which clearly shows exponential decay curvature, i.e. the longer the residence times, the fewer number of cases are detected.

In order to assess the dynamic aspect of the first hydration shell, maximum and average residence times, *Tr*, for all water molecules in the first hydration shell ($R < 3.5$ Å) around specified solute atoms can be calculated. The results listed in Table 1 reveal differences in the average residence times ranging from 0.32 ps around O-1′ (sucrose) to 0.69 ps around O-2 and O-2′ (trehalose) and around O-3f (sucrose). The estimated standard deviations for the average residence times are approximately 0.002 ps. In the average calculation, the acetal and hydroxyl oxygens clearly display different hydration dynamics, but the left side and the right side hydroxyl groups (Fig. 8) in sucrose also display significantly different hydration dynamics consistent with the hydration densities. On the 'right side' of sucrose

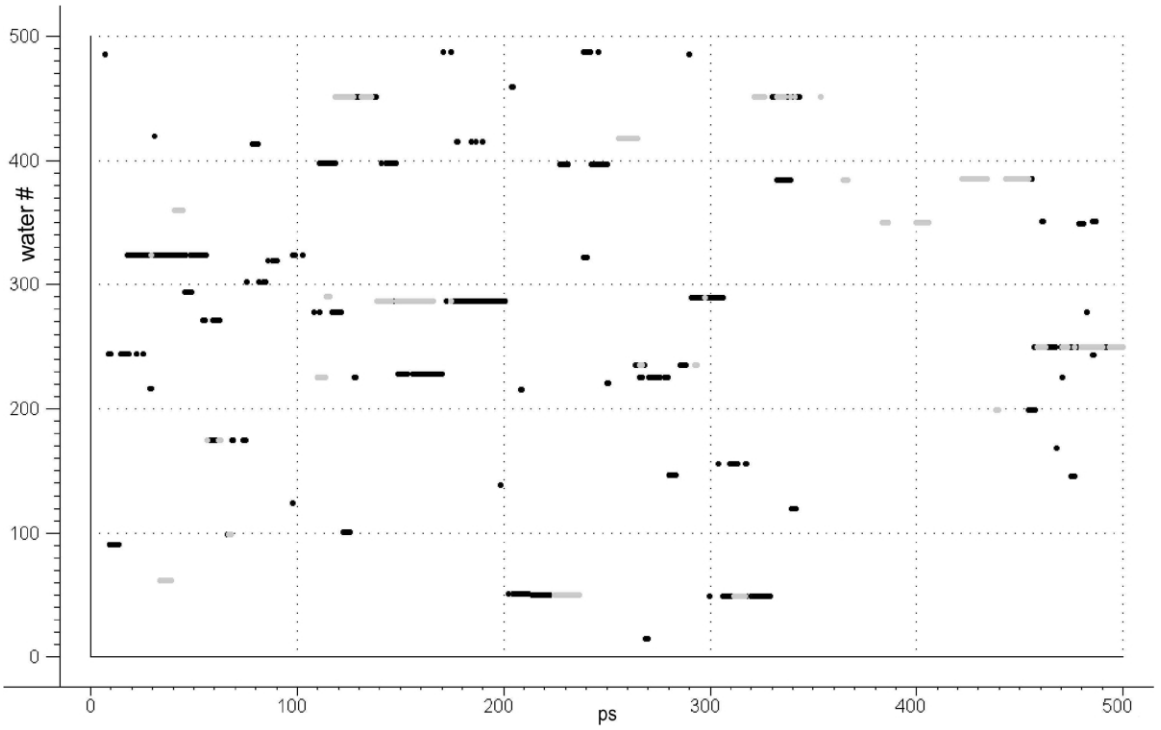

Fig. 9. Intersection events for the various water molecules. The event of being in the first hydration shell intersection of O-2g and O-1f (blue) and the event of being in the first hydration shell intersection of O-2g and O-3f (red) for a water molecule (oxygen) recorded as a function of trajectory time (10^{-11} s).

(Fig. 8), the residence times are comparable to those in pure water. However, the short average residence times indicate that it is not the large flux through the more voluminous outer parts of the first hydration shell that is the dominant hydration feature. The variations in the maximum residence times reflect the same trend with O-2 in sucrose as a notable exception. Water–water interactions exhibit slightly longer residence times in the trehalose trajectory: 0.552(2) ps compared with 0.544(2) ps for the sucrose trajectory. They also appear to reflect a lower water mobility in trehalose solutions (vide supra; Table 4). From Table 1 it is evident that the very long residence times at approximately O-2 and O-2′ is a significant feature of trehalose hydration, while for sucrose long residence times are observed in the vicinity of O-3′ and O-2. In reality, the number of occurrences of a water molecule residing as a function of residence time, *Tr*, is an exponentially decreasing population. In our analysis this exponential decay displays clear bi-exponential behaviour (Fig. 12): (i) a large population (93–99%) of a very rapidly decaying component with a characteristic residence time, *Tr1*, of 0.5–0.6 ps, much in line with bulk water dynamics; and (ii) a small population (1–7%) of a more slowly decaying component, *Tr2*, with a characteristic residence time in the range of 1.3–3.1 ps. Again for trehalose we observe that O-2 and O-2′ have the longest residence times, 2.7 and 3.0 ps, respectively, while sucrose O-2g and O-1f has the longest residence time (the *Tr1* for O-5′ does not appear to be a robust estimate in this analysis). In conclusion, residence times appear not to provide convincing evidence for identification of special hydration sites. Calculation of (hindered) rotational diffusion for the first hydration shell waters

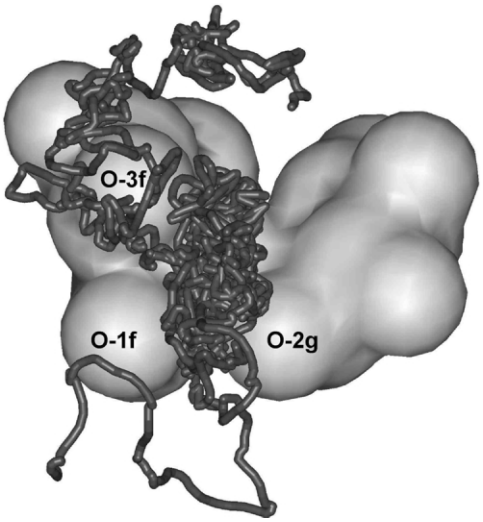

Fig. 10. Eighty-picosecond trajectory of water molecule (black) superimposed on the heavy-atom van der Waals surface of sucrose. Adapted from Engelsen [47].

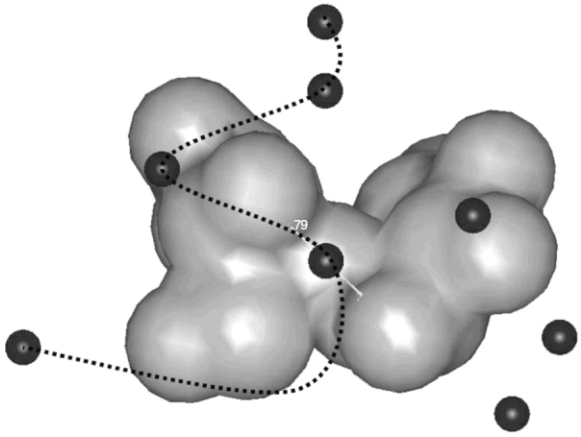

Fig. 11. The hydration of one sucrose molecule in the binding site of a lentil lectin possessing an inter-ring water bridge between O-2g and O-3f. Note the similarity to Fig. 10. Adapted from Engelsen [47].

would appear to be a better indicator, but much longer trajectory times would be required to obtain acceptable statistics.

5.4. Diffusion

When water is added to a molecular dynamics trajectory it adds new properties to the solute namely rotational diffusion and translational diffusion. The self-diffusion of the solute can be obtained via the Einstein relation by calculating the centre of mass mean square displacement autocorrelation: $D(\Delta t) = \langle |\vec{r}(t + \Delta t) - \vec{r}(t)|^2 \rangle / 6\Delta t$ which becomes valid for long Δt. Using this equation a diffusion coefficient of 5.0–5.5 10^{-6} cm^2

Table 1
Average (T_{av}) and maximum (T_{max}) residence times (in picoseconds) for water molecules in the first hydration shell around solute oxygens ($R < 3.5$ Å)

Atom	Sucrose				Trehalose			
	Tr_{max}	Tr_{av}	Tr_1	Tr_2	Tr_{max}	Tr_{av}	Tr_1	Tr_2
O-1g/O-1	9.4	0.41	0.46	2.0 (3)	17.26	0.32	0.50	2.2 (1)
O-2g/O-2	15.0	0.68	0.56	3.0 (3)	27.20	0.69	0.53	2.7 (4)
O-3g/O-3	18.2	0.64	0.56	2.3 (6)	19.28	0.64	0.56	2.5 (5)
O-4g/O-4	18.1	0.64	0.57	2.7 (4)	17.54	0.61	0.56	2.2 (5)
O-5g/O-5	13.3	0.46	0.52	2.6 (2)	10.18	0.37	0.46	1.5 (5)
O-6g/O-6	17.2	0.60	0.61	2.2 (5)	18.54	0.61	0.58	2.5 (4)
O-1f/O-2′	20.2	0.63	0.58	2.8 (3)	23.02	0.69	0.53	3.0 (3)
O-3f/O-3′	30.6	0.69	0.53	2.5 (5)	16.60	0.66	0.56	2.5 (5)
O-4f/O-4′	12.6	0.58	0.55	2.0 (5)	16.82	0.62	0.56	2.3 (5)
O-5/O-5′	11.7	0.39	0.58	3.1 (1)	8.02	0.36	0.49	1.3 (7)
O-6f/O-6′	15.7	0.58	0.47	1.7 (1)	22.40	0.61	0.60	2.4 (5)
Ow...Ow	24.8	0.54			29.38	0.55		

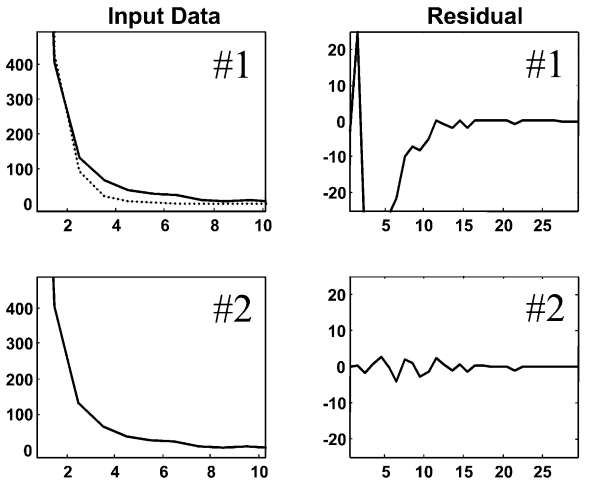

Fig. 12. Water residence time distribution profile (O-3f sucrose). It is clear that the profile contains two populations: one quickly repulsed population and a more resident population (approx. 5%) with a characteristic decay time of 2.5 ps. The red curve is the population curve and the blue curve is the exponential fit curve.

s^{-1} for sucrose in water can be deduced, in good agreement with the experimental determination listed to be 5.21×10^{-6} cm^2 s^{-1} for a 0.38% (w/w) solution at 298 K (52nd edition of the *Handbook of Chemistry and Physics*). The calculated translational diffusion of trehalose from molecular dynamics simulation was approximately $5.0–5.2 \times 10^{-6}$ cm^2 s^{-1} and thus similar to that of sucrose which is in good agreement with the fact that at low concentrations the translational diffusion of the four non-reducing disaccharides: sucrose, allosucrose, leucrose and α,α-trehalose are quite similar [49]. Analogous calculations on maltose [7] have been performed, yielding somewhat less convincing results, in part due to much shorter trajectories.

The rotational diffusion, or overall tumbling, can be assessed in an analogous manner to the translational diffusion. In this case, a descriptive molecular vector is needed, e.g. the dipole moment [4]. The overall molecular tumbling time for the solute can then be estimated from the angular evolution of the solute dipole moment, as expressed by the autocorrelation function for the angular displacement of the dipole moment vector. In the sucrose case the angular information is uncorrelated after approximately 110–140 ps, in good agreement with the experimental value of 120 ps [14]. In contrast, the rotational diffusion of trehalose as calculated from molecular dynamics simulations appears to be significantly slower than for sucrose. The latter feature appears to be in good accordance with the experimental differences where the overall correlation time as derived from NMR experiments by Batta et al. [39] was estimated in the range of 400–500 ps.

6. NMR and carbohydrate hydration

6.1. Background on NMR hydration studies

NMR investigations of the hydration water molecules interacting with a biological macromolecule have been based on three types of data [50,51]: (i) the longitudinal and transverse relaxation of water molecules; (ii) ^{17}O-NMR shielding constants that are very sensitive to hydrogen bonding interactions; and (iii) intermolecular NOEs stemming from specific solute–solvent interactions. In the case of proteins, at least three broad classes of water molecules have been distinguished on T_1 criteria and the corresponding rotational correlation times: (i) bulk water (τ_C = 10 ps or less); (ii) 'translationally-hindered water' (τ_C in the nanosecond range); and (iii) irrotationally bound water (the same τ_C as that of the macromolecules, 10 μs to 10 ns or less). In the most successful model for describing NOE-defined hydration interactions ('the translational diffusion model') [52], random and independent translation and rotation of both the macromolecule and the water molecules were considered. The diffusion coefficients were translated into residence times of the hydration water molecules using the relation ($\tau = \chi^2/D_t$) derived from the Einstein–Smoluchowski equation. The size of intermolecular NOEs and ROEs between water and the macromolecules and, more importantly, their sign were shown to be sensitive to residence times in the nanosecond range. The lower limit for probing water residence times with intermolecular NOEs and ROEs can be esti-

mated to be approximately 10 ps, as for shorter values the dipolar contribution to relaxation is too small to be detected.

In the case of dilute solutions of carbohydrates, the very low sensitivity (due to an unfavourable magnetogyric ratio as well as low natural abundance) of ^{17}O-NMR in the absence of isotope labelled compounds precludes widespread use in hydration studies. Although low temperature studies of carbohydrates in water have been developed in Kenne's group [53] to take advantage of hydroxyl proton interactions, to date, they have not been able to detect intermolecular NOEs between sugar methine protons and the solvent (personal communication), possibly owing to very short residence times that are revealed by molecular dynamics trajectories. As a result, the most promising NMR approach to the hydration of carbohydrates resides in systematic studies of rotational (obtained from relaxation data) [54] and translational (extracted from pulsed-field gradient spin-echo experiments, PFGSE) [55] diffusion of both sugars and water as a function of both temperature and concentration but few investigations of dilute solutions have been reported. The problems associated with hydrodynamic studies of carbohydrates and with the NMR approaches will be briefly reviewed before considering preliminary results in this area.

6.2. Hydrodynamic theory of rotational and translational diffusion

Hydrodynamic modelling of biological macromolecules has been a fruitful field of research and formalisms are available for expressing both the rotational and translational diffusion of molecules with various distinctive molecular shapes [56–58]. Conversely, for rigid molecules of known shape, molecular dimensions can be established from experimental D_t or D_r coefficients. This approach has not been widely used in studies of medium-sized molecules due to the need of ambiguous empirical microviscosity correction factors, f [59,60]. Indeed, when the target molecule is approximately the same size as the solvent molecules (slip regime), f can vary over more than an order of magnitude ($0 < f < 1$) and depends on both molecular size and shape. A recent systematic study of the translational diffusion of dilute solutions of carbohydrates as a function of size has shown that classical Stokes behaviour (stick regime where the solvent can be treated as a continuum described by bulk viscosity) prevails for oligosaccharides the size of a tetrasaccharide or larger [61]. This conclusion was based on comparison of the molecular dimensions of theoretical models of the carbohydrates (exhaustive molecular modelling investigations had been reported for all of the sugars described in this work) with those established from translational diffusion coefficients, D_t, using hydrodynamic theory. Thus, the behaviour of dilute solutions of disaccharides cannot be probed in a quantitative manner, as the microviscosity correction factor is in the 0.75–0.80 range. This conclusion is in agreement with pioneering optical studies on the hydrodynamic properties of carbohydrates that focused on the influence of concentration and temperature on the translational diffusion coefficients (D_t) of aqueous solutions of mono- and disaccharides [62–65]. Deviations from Stokes–Einstein behaviour were interpreted in terms of disruption of local water structure around the sugars, and an empirical relationship to the number of equatorial hydroxyl groups was proposed [66–68].

The other fundamental problem associated with quantitative analysis of hydrodynamic data is molecular flexibility and this obstacle is particularly important in the case of carbohydrates. In the aforementioned systematic study of carbohydrate D_t data as a function of molecular size, all of the major conformational families from the theoretical investigations were considered when establishing the molecular dimensions from the ensembles of privileged geometries. Ideally, either molecular volume or the diffusion tensors themselves should be averaged over all conformational space and this leads to a very debatable point concerning the precise definition of hydrodynamic volume. In other words, what should the distance between the extremity of the van der Waals radii of peripheral hydroxyl hydrogens (usually the outermost atoms) with respect to water molecules really be in the case of sugars?

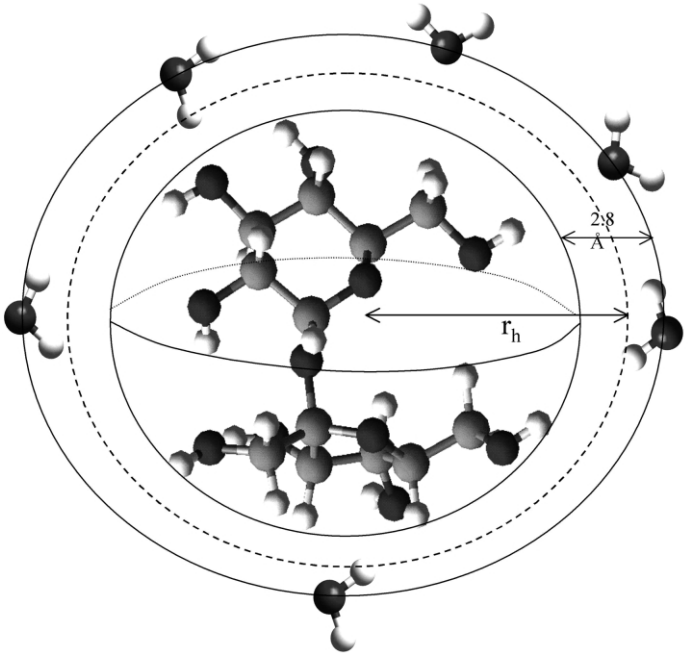

Fig. 13. The hydrodynamic model for sucrose.

The definition used in the PFGSE study of carbohydrates, [61] based on radial pair distributions calculated for molecular dynamics trajectories of disaccharides in explicit solvent, is illustrated in Fig. 13, but theoretical developments in this area would obviously be timely.

6.3. PFGSE-defined D_t data of carbohydrates

Drug design has motivated the development of diffusion-edited NMR spectroscopy [69] that permits the screening of compound libraries based on the differences in observed translational diffusion coefficients, D_t, between binding and non-binding components [69–74]. These experiments rely on the accurate measurement of the self-diffusion coefficients of small molecules with spin-echo sequences using pulsed field gradients (PFGSE) [55]. Indeed, with the advent of modern NMR spectrometers equipped with units that produce well-defined pulsed-field gradients (PFG), D_t can be measured very rapidly. The underlying principle behind PFGSE experiments is very simple: transverse magnetisation is created with a 90° hard pulse, a first pulsed field gradient across the sample induces macroscopic dephasing of this transverse magnetisation, and it is subsequently rephased with a second pulsed field gradient. In the absence of translational diffusion these sequences work like classical spin-echo sequences rephasing (instead of refocusing) transverse magnetisation. Translational diffusion of the target molecule results in incomplete rephasing and the resulting echo attenuation is proportional to the field gradient G (gauss/cm), its duration, the magnetogyric ratio of the detected nucleus, γ, its D_t coefficient and certain experimental parameters (delays in the pulse sequence), if the relaxation contribution is ignored. The technical aspects regarding these experiments have been reviewed elsewhere but in the case of carbohydrates two points should be emphasised. It is necessary to take transverse relaxation into account in the fitting of data to the Stejskal–Tanner equation and it is desirable to calibrate the strength of the

gradient field with respect to several compounds with known D_t coefficients (pure water for example) as opposed to calibration through bandwidth analysis in a steady field gradient. Molecular volumes estimated from PFGSE-determined D_t coefficients are generally overestimated due to overattenuation of the echo signal (resulting from eddy currents, convection currents, non-linearity of the gradient across the sample, etc.).

To date, D_t coefficients of carbohydrates established with the PFGSE approach [49,74–79] have been undertaken: (i) to validate the theoretical self-diffusion coefficients calculated from MD trajectories [76,78]; (ii) to demonstrate the complexation of lanthanide cations by sugars [74]; (iii) to probe the geometry of a molecular capsule formed by electrostatic interactions between oppositely-charged β-cyclodextrins [77]; (iv) to study the influence of concentration and temperature dependence on the hydrodynamic properties of disaccharides [49]; and (v) to discriminate between extended and folded conformations of nucleotide-sugars [79].

6.4. NMR-defined rotational diffusion

Rotational diffusion, D_r, can be probed by a variety of NMR experiments, as this mode of Brownian motion modulates relaxation processes. In most cases theoretical spectral densities (expressed in terms of the rotational correlation time, τ_C, with $D_r = 1/6\tau_C$) that correspond to various motional models are fitted to experimental data (heteronuclear T_1, T_2 and NOE [54], CSA/DD cross-correlation [39], off-resonance experiments [80], etc.) while considering the parameters of the motional model as adjustable parameters. The most popular motional model for oligosaccharides relies on Lipari and Szabo's model-free spectral densities [81] for either isotropic or axially symmetric anisotropic overall motion. Formalisms that allow one (fast) or two (both fast and slow internal motion) modes for internal fluctuations have been proposed [82]. The amplitude of internal motion is characterised by the angular order parameter that varies from 1.0 for a totally rigid molecule to 0.0 for a totally flexible molecule. In the case of heteronuclear relaxation data for methine carbons where the carbon–proton distance can be considered to be fixed (r_{CH} values between 1.09 and 1.12 Å are widely used [83], but this Δr_{CH} corresponds to a $\Delta\tau_C$ of approx. 10%) the fitting of multi-field data does not provide a unique solution, but rather a continuum of models (during fitting an increase in the amplitude of the internal motion is compensated by a concomitant increase in the correlation times for the overall motion).

Similarly, a superposition of factors (geometry and chemical shift anisotropy) is obtained with the recently proposed measurement of chemical shift anisotropy from the DD/CSA cross-correlated spectral densities, and an independent estimation of molecular tumbling was obtained with a 'trouble-free' variable temperature approach [39]. In contrast, off-resonance experiments [80] afford a unique solution for the motional behaviour of a given pair of spins, but these experiments are time-consuming and the information must ultimately be translated into a motional model to be meaningful. Alternatively, either the angular order parameters [84] or the time correlation functions (TCFs) themselves can be calculated directly from the MD trajectories [85] and then used to establish theoretical data that are compared with experimental ones. The approximations inherent in these approaches concern the averaging methods that have supposed that all of the pertinent time-scales are well-separated and that the angular and radial contributions to the internal motion can be separated.

In spite of the aforementioned approximations, rotational motional models for simple carbohydrates converge to give a fairly small range of order parameters and correlation times. In the following preliminary NMR probe of hydration, the hydrodynamic behaviour of three model disaccharides that have been extensively studied with MD simulations in dilute aqueous solution has been evaluated through D_t and D_r data. Average values for the D_t coefficients of the solvent have been determined and interpreted in terms of a simplified view of hydration.

Table 2
Carbon T_1 (125 MHz) values of maltose and trehalose in dilute (4% w/w) aqueous solutions at 298 K and heteronuclear NOE factors (100 MHz), η of the aforementioned sample of trehalose

Carbohydrate residue	Relaxation parameter	C-1	C-2	C-3	C-4	C-5	C-6	Average value
α-*Maltose*								
α-Glc*p*-(1 → 4)	T_1	0.56 (±0.02)	0.54 (±0.02)	0.54 (±0.01)	0.52 (±0.02)	0.54 (±0.01)	0.31 (±0.02)	0.54
α-Glc*p*-OH	T_1	0.51 (±0.02)	0.62 (±0.01)	0.61 (±0.02)	0.57 (±0.02)	0.61 (±0.02)	0.31 (±0.02)	0.58
β-*Maltose*								
α-Glc*p*-(1 → 4)	T_1	0.52 (±0.01)	0.51 (±0.008)	0.52 (±0.01)	0.52 (±0.01)	0.51 (±0.03)	0.32 (±0.01)	0.52
β-Glc*p*-OH	T_1	0.66 (±0.01)	0.63 (±0.01)	0.62 (±0.01)	0.58 (±0.01)	0.62 (±0.01)	0.29 (±0.01)	0.62
α-*Trehalose*	T_1	0.483 (±0.003)	0.479 (±0.003)	0.490 (±0.005)	0.495 (±0.005)	0.499 (±0.004)	0.294 (±0.004)	0.489
	η	1.13	1.08	1.04	1.09	0.97	1.204	

6.5. Experimental D_r and D_t coefficients for 4% w/w aqueous solutions of three disaccharides

The 125 MHz carbon T_1 data for 4% w/w aqueous solutions of maltose and α,α-trehalose at 298 K are compiled in Table 2. Extensive carbon relaxation data have been reported for sucrose [14,83] but for comparative purposes the T_1 data acquired under the most analogous conditions (296 K, 4% w/w) [14] were used to establish the correlation time for rotational diffusion, τ_C. In the earlier study [14], a 120-ps correlation time (instead of the 200–270-ps range indicated in Table 3) was reported and this was the result of fitting the relaxation data with both a shorter r_{CH} value and a different motional model. Similarly, Batta et al. reported a very short τ_C-value for an infinitely dilute solution of α,α-trehalose (100 ps) but again for comparative purposes (i.e. both identical experimental and simulation conditions) the parameter range indicated in Table 3 will be retained for discussion. It should be remarked that fairly small spreads in T_1-values and in carbon NOE factors for the

Table 3
Rotational (T_1 defined) and translational (PFGSE) diffusion coefficients of carbohydrates in dilute solutions of carbohydrates in D_2O[a] at 298 K

Carbohydrate	Rotational diffusion				Translational diffusion	
	Model A		Model B		D_t	Sphere
	τ_C (ps)	Sphere (rÅ)	τ_C (ps)	Sphere (rÅ)	(10^{-6} cm^2 s^{-1})	(rÅ)
α-Maltose	190	5.5	250	6.1	4.04 ± 0.01	5.0
Sucrose	200	5.6	270	6.2	4.30 ± 0.05	4.7
Trehalose	240[b]	6.0	350[c]	6.8	3.93 ± 0.07	5.1

Key: rigid rotor, Model A (order parameter 0.9, τ_ι 50 ps); flexible rotor, Model B (order parameter 0.7, τ_ι 50 ps).
[a] Viscosity ratio $\eta_{D_2O}/\eta_{H_2O} = 1.23$.
[b] Simulation of η with Model A gives a τ_C-value of 285 ps.
[c] Simulation of η with Model B gives a τ_C-value of 290 ps.

various methine carbons of these three carbohydrates indicate that overall tumbling is almost isotropic. This justifies the use of isotropic spectral density functions to establish the correlation times for rotational diffusion, τ_C, from the T_1 data that are given in Table 2. Similar τ_C-values were obtained for trehalose when the carbon NOE factors were simulated with isotropic spectral densities and these parameters are less sensitive to internal dynamics for small molecules like disaccharides (see footnote to Table 3).

The translational diffusion of 4% w/w aqueous solutions of these three disaccharides have been measured with the STE pulse sequence [86] and the D_t coefficients are also compiled in Table 3. It is to be noted that the gradient field was initially calibrated with respect to the bandwidth of the water signal in a steady gradient and therefore all the D_t coefficients were divided by 0.82 to achieve calibration with respect to the known diffusion coefficient of water in D_2O (a value of 15.3 instead of 18.7×10^{-6} cm^2 s^{-1} was measured on the 400-MHz spectrometer). Using this latter calibration protocol leads to almost identical D_t coefficients for sucrose and maltose as those reported by Uedaira and Uedaira [66–68] based on optical measurements.

The radii of the spheres encasing the three disaccharides have been established from both the rotational and translational data using the Debye and Stokes–Einstein relation, respectively [Eqs. (2) and (3) where k is Boltzmann's constant, T the temperature in K, and η_0 is the viscosity of the solvent]. Kinematic viscosity measurements of the 4% w/w aqueous sugar solutions at 298 K revealed flow almost identical to that of pure water, so that the viscosity of water (D_2O) [87] was used in the preceding equations without correction. It can be seen that the motional model used for interpreting the rotational diffusion influences the 'experimental' molecular radii ($\Delta r \sim$ 0.6–0.8 Å for Models A and B in Table 3). Although the molecular radii obtained from rotational (Model A) and translational diffusion appear to agree reasonably well ($\Delta r < 1$ Å), this parameter is clearly not determined with sufficient accuracy to 'see' an irrotationally-bound water molecule.

The average atom-to-atom molecular radii established from the atom-to-atom dimensions of the preferred conformers (average value for the various minimum-energy geometries) of the three sugars are 5.2, 4.7 and 4.6 Å, respectively, for α-maltose, sucrose and α,α-trehalose. These values should be increased by between 0.9 and 1.4 Å to prevent inter-penetration of the van der Waals radii of the solvent and sugar atoms (see Fig. 13) based on the Ow/Os radial pair distribution functions established from MD trajectories ($d_{Ow/Os} \sim 2.8$ Å). This definition of the hydrodynamic radius that excludes the first water shell around the sugars corroborates the need for a microviscosity correction factor of approximately 0.75–0.80 in Eq. (3) to obtain reasonable agreement between molecular model-based molecular dimensions and the NMR-derived dimensions in Table 3.

$$\tau_C = 4\pi r \eta_0 / 3kT \tag{2}$$

$$D_t = kT / 6\pi r \eta_0 \tag{3}$$

In Table 4 we have collected the translational diffusion coefficients of water for the 4% w/w solutions of maltose, sucrose and trehalose in H_2O (the data have been scaled up so that the D_t coefficients of pure water at both magnetic fields are 23×10^{-6} cm^2 s^{-1}). As regards the 4% w/w samples (489 water molecules per sugar molecule as was the case in the MD trajectories), it can be seen that the experimental precision of the D_t coefficients is undoubtedly sufficient (all three D_t coefficients for the water in the 4% w/w solutions were measured at least twice) to show that the water molecules in the first hydration shell (roughly 30 out of the 489 molecules present) are not irrotationally bound to the sugar molecules (for example, the observed D_t coefficients of the water in the sucrose solution is identical to that of bulk water rather than the value of 21.9×10^{-6} cm^2 s^{-1} expected with the following calculation).

$$\{(489 - 30) * D_t(\text{bulk water}) + (30) * D_t(\text{first hydration shell})\}/489 = D_t(\text{observed})$$

Table 4
Translational diffusion coefficients of water in dilute solutions of carbohydrates at 298 K measured at 400[a] or 500[b] MHz with the pulsed field gradient spin echo technique

Carbohydrate	[C] (w/w%)	Global D_t 10^{-6} cm^2 s^{-1}
Maltose	4	23.1 ± 0.01[b]
	10	21.8 ± 0.05[a]
Sucrose	4	24.1 ± 0.05[b]
	10	22.2 ± 0.05[a]
Trehalose	4	24.7 ± 0.06[a]
	10	21.4 ± 0.01[b]
H_2O	Pure	23.0 ± 0.02[a]
		23.0 ± 0.06[b]

As stated previously, viscosities of the 4% w/w samples were measured and are almost identical to that of pure water. Concerning the 10% w/w samples, the decrease in the observed D_t coefficients of the water reflect both an increase in viscosity and structuring of water around the sugar molecules. Thus, in the case of very dilute solutions analysis of water translational diffusion corroborates the hydrodynamic radius of the sugar molecule proposed in Fig. 13 (i.e. r_h does not include the first shell of water molecules).

7. Conclusions

The dilute hydration of carbohydrate model substances shows remarkable differences. Of two molecules thoroughly investigated by comparative molecular dynamics techniques and high resolution NMR techniques sucrose and trehalose are found to display significant changes upon solvation in very good agreement with NMR measures. However, their detailed hydration is found to be very different. A localised very strong hydration site is found to be a major feature of sucrose hydration, and this is accompanied by a distribution of solvent molecules that display a high degree of anisotropy. Other cases of solvent anisotropy have been reported [88] for monosaccharides, explaining that β-anomers of D-xylopyranose and D-glucopyranose predominate in aqueous solution in spite of quantum mechanics prediction that the α-anomer should be preferred. Trehalose does not display a strong localised hydration site, but the comparison between dilute solution and solid-state reveals trehalose to be almost perfectly hydrated in the crystalline dihydrate environment. It is, however, important to stress that molecular simulations without explicit water molecules would not have detected the oblong water cavity of prime importance to sucrose hydration, nor would the trehalose asymmetry have been observed. To obtain a better understanding of the dynamic and static interactions between carbohydrates and water, one of the only feasible routes is by performing molecular dynamics simulations with explicitly present water molecules.

Complementary to the computational tools, this review offers a clear presentation of our current state of knowledge of using NMR-derived data to decipher key structural and dynamical features of carbohydrates by which we can distinguish between three classes of water molecules depending on their rotational correlation times. These provide conceptual framework to further characterise key hydration of carbohydrates in conjunction with indications derived from MD simulations. Our preliminary reports on the variations of hydration characteristics as a function of concentration certainly open pathways toward more experimental studies that are required in conjunction with parallel computational work performed under similar conditions.

We believe that all the analytical tools that have been developed to extract significant descriptors for the hydration can be used in a much more general characterisation of the hydration features occurring both at the solute level and the solvent level. These tools can be made available for any detailed MD investigations of other carbohydrate molecules, providing that simulation, long enough in time to be statistically meaningful, is carried out.

Obviously the number of well-documented studies, both from the simulation point of view and the experimental one, is far from sufficient to render a definite understanding of the hydration

of carbohydrate molecules. There is absolutely no reason to expect to achieve a thorough understanding of the hydration features of carbohydrates from only two documented examples. We can only hypothesise that a myriad of different situations could be occurring as the majority of direct hydrogen bonding interactions between carbohydrates and aqueous solvent are through hydroxyl groups. These moieties behave very much like the water molecules themselves in their hydrogen bonding, but the numerous configurational states that carbohydrate molecules offer are likely to generate a plethora of structural and dynamical states that will result in subtle or drastic perturbations of the surrounding water medium and subsequently induce functionality.

It has not escaped our attention that the relevance of this endeavour to explain functional properties of carbohydrates may also involve the understanding of their hydration features in a more concentrated state. While we can maintain that a reasonable understanding is being achieved for either the extremely dilute state or the highly ordered condensed state as found in the crystalline state, the intermediate cases are more likely to be relevant for explaining either functional properties or biological roles.

8. Experimental section

8.1. NMR

^{1}H-NMR pulsed-gradient spin-echo experiments (PGSE) were conducted on either a Bruker DRX 400 or a Bruker DRX 500 spectrometer at 298 K. The stimulated spin-echo sequence [86] was used to measure the translational self-diffusion coefficients. The gradient duration (δ) was varied from 1 to 20 ms while keeping its strength fixed at 9.15 (9.9) G/cm for the 400 (500) MHz experiments. The intergradient delay (Δ) was chosen to be as short as possible while affording the maximum signal intensity for the shortest τ-value. The translational self-diffusion coefficients have been obtained by fitting the intensities of a selected proton signal in spectra acquired with various lengths of the gradient pulses (8–15 data points) to the Stejskal–Tanner equation with in-house software:

$$M = \frac{1}{2} M_0 \exp\Big\{ -(\tau_2 - \tau_1)/T_1 - 2\tau_1/T_2 - \Big((\tau_1 G\gamma)^2 D_t(\tau_2 - (\tau_1/3))\Big)\Big\}$$

Several proton signals were monitored in separate experiments to estimate the experimental error in the estimation of D_t and all experiments were run at least twice.

Proton and carbon spin-lattice relaxation times were measured with the inversion-recovery sequence. The recycle time was greater than $6 \times T_1$ and data were collected for 10–20 τ values which varied from 5 ms to $2 \times T_1$. Proton spin–spin relaxation times were obtained with the Carr–Purcell–Meiboom–Gill sequence and data were collected for roughly 20 spectra with various numbers of echoes (2 ms to 1 s). Carbon nuclear Overhauser factors, η, were obtained by quantifying the carbon integrals in both composite-pulse decoupled and inverse-gated spectra. The integrals of the peaks were fitted to a three- (T_1) or two- (T_2) parameter exponential function using both spectrometer system software and in-house software and all experiments were run at least twice.

Acknowledgements

S.B.E. was supported by the Centre of Advanced Food Studies (LMC) in a project concerning molecular modelling of carbohydrates and C.M. benefited from a Ph.D. scholarship from the French Ministry of Education and Research.

References

[1] K. Bock, R.U. Lemieux, The conformational properties of sucrose in aqueous solution: intramolecular hydrogen-bonding, Carbohyd. Res. 100 (1982) 63–74.
[2] J.R. Grigera, Conformation of polyols in water: molecular-dynamics simulations of mannitol and sorbitol, J. Chem. Soc. Perkin Trans. 1 84 (1988) 2603–2608.
[3] J.H.E. Koehler, W. Saenger, W.F. van Gunsteren, Conformational differences between alpha-cyclodextrin in

aqueous solution and in crystalline form. A molecular dynamics study, J. Mol. Biol. 203 (1) (1988) 241–250.
[4] J.W. Brady, Molecular dynamics simulations of α-D-glucose in aqueous solution, J. Am. Chem. Soc. 111 (1989) 5155–5165.
[5] B.P. van Eijck, J. Kroon, Molecular-dynamics simulations of β-D-ribose and β-D-deoxyribose solutions, J. Mol. Struct. 195 (1989) 133–146.
[6] P.J. Rossky, M. Karplus, Solvation. A molecular dynamics study of a dipeptide in water, J. Am. Chem. Soc. 101 (8) (1979) 1913–1937.
[7] J.W. Brady, R.K. Schmidt, The role of hydrogen bonding in carbohydrates: molecular dynamics simulations of maltose in aqueous solution, J. Phys. Chem. 97 (4) (1993) 958–966.
[8] K.-H. Ott, B. Meyer, Molecular dynamics simulations of maltose in water, Carbohyd. Res. 281 (1996) 11–34.
[9] C.J. Edge, U.C. Singh, R. Bazzo, G.L. Taylor, R.A. Dwek, T.W. Rademacher, 500-picosecond molecular dynamics in water of the Manα1–2Manα glycosidic linkage present in asn-linked oligomannose-type structures on glucoproteins, Biochemistry 29 (1990) 1971–1974.
[10] B.A. Spronk, A. Rivera-Sagredo, J.P. Kamerling, J.F. Vliegenthart, A reinvestigation towards the conformation of methyl alpha-D-mannopyranosyl-(1 → 6)-alpha-D-mannopyranoside by a combined ROE and molecular dynamics analysis, Carbohyd. Res. 273 (1995) 11–26.
[11] L.M.J. Kroon-Batenburg, J. Kroon, B.R. Leeflang, J.F.G. Vliegenthart, Conformational analysis of methyl β-cellobioside by ROESY NMR spectroscopy and MD simulations in combination with the CROSREL method, Carbohyd. Res. 245 (1993) 21–42.
[12] S. Immel, F.W. Lichtenthaler, The conformation of sucrose in water: a molecular dynamics approach, Liebigs Annalen (1995) 1925–1937.
[13] S.B. Engelsen, S. Pérez, The hydration of sucrose, Carbohyd. Res. 292 (1996) 21–38.
[14] S.B. Engelsen, C. Hervé du Penhoat, S. Pérez, Molecular relaxation of sucrose in aqueous solution: how a nanosecond molecular dynamics simulation helps to reconcile NMR data, J. Phys. Chem. 99 (1995) 13334–13351.
[15] K. Ueda, J.W. Brady, The effect of hydration upon the conformation and dynamics of neocarrabiose, a repeat unit of beta-carrageenan, Biopolymers 38 (1996) 461–469.
[16] M.C. Donnamaria, E.I. Howard, J.R. Grigera, Interaction of water with α,α-trehalose in solution: molecular dynamics approach, J. Chem. Soc. Faraday Trans. 90 (18) (1994) 2731–2735.
[17] Q. Liu, R.K. Schmidt, B. Teo, P.A. Karplus, J.W. Brady, Molecular dynamics studies of the hydration of α,α-trehalose, J. Am. Chem. Soc. 119 (1997) 7851–7862.
[18] S.B. Engelsen, S. Pérez, Unique similarity of the asymmetric trehalose solid-state hydration and the diluted aqueous-solution hydration, J. Phys. Chem. B 104 (39) (2000) 9301–9311.
[19] J.H. Crowe, L.M. Crowe, D. Chapman, Preservation of membranes in anhydrobiotic organisms: the role of trehalose, Science 223 (1984) 701–703.
[20] L.M. Crowe, R. Mouradian, J.H. Crowe, S.A. Jackson, C. Womersley, Effects of carbohydrates on membrane stability at low water activity, Biochim. Biophys. Acta 947 (1984) 367–384.
[21] IUPAC-IUB nomenclature of carbohydrates, Carbohyd. Res. 297 (1997) 1–92.
[22] G.M. Brown, H.A. Levy, Further refinement of the structure of sucrose based on neutron-diffraction data, Acta Cryst. B 29 (1973) 790–797.
[23] M.E. Gress, G.A. Jeffrey, A neutron diffraction refinement of the crystal structure of β-maltose monohydrate, Acta Cryst. B 33 (1977) 2490–2495.
[24] T. Taga, M. Senma, K. Osaki, The crystal and molecular structure of trehalose dihydrate, Acta Cryst. B 28 (1972) 3258–3263.
[25] G.M. Brown, D.C. Rohrer, B. Berking, C.A. Beevers, R.O. Gould, R. Simpson, The crystal structure of α,α-trehalose dihydrate from three independent X-ray determinations, Acta Cryst B 28 (1972) 3145–3158.
[26] G.A. Jeffrey, R. Nanni, The crystal structure of anhydrous α,α-trehalose at −150°, Carbohyd. Res. 137 (1985) 21–30.
[27] F. Takusagawa, R.A. Jacobson, The crystal and molecular structure of α-maltose, Acta Cryst. B 34 (1978) 213–218.
[28] B.J. Alder, T.E. Wainwright, Studies in molecular dynamics. I. General method, J. Chem. Phys. 31 (1959) 459.
[29] F.H. Stillinger, A. Rahman, Improved simulation of liquid water by molecular dynamics, J. Chem. Phys. 60 (4) (1974) 1545–1557.
[30] W.F. van Gunsteren, H.J.C. Berendsen, Algorithms for macromolecular dynamics and constraint dynamics, Mol. Phys. 34 (5) (1977) 1311–1327.
[31] W.F. van Gunsteren, M. Karplus, Effects of constraints on the dynamics of macromolecules, Macromolecules 15 (1982) 1528.
[32] C.L. Brooks III, A. Brünger, M. Karplus, Active site dynamics in protein molecules: a stochastic boundary molecular-dynamics approach, Biopolymers 24 (1985) 843.
[33] S. Pérez, A. Imberty, S.B. Engelsen et al., A comparison and chemometric analysis of several molecular mechanics force fields and parameter sets applied to carbohydrates, Carbohyd. Res. 314 (1998) 141–155.
[34] W.L. Jorgensen, J. Chandrasekhar, J.D. Madura, R.W. Impey, M.L. Klein, Comparison of simple potential functions for simulating liquid water, J. Chem. Phys. 79 (2) (1983) 926–935.
[35] S.N. Ha, A. Giammona, M. Field, J.W. Brady, A revised potential-energy surface for molecular mechanics of carbohydrates, Carbohyd. Res. 180 (2) (1988) 207–221.
[36] S.Q. Sheng, H. van Halbeek, Evidence for a transient interresidue hydrogen bond in sucrose in aqueous solu-

tion obtained by rotating-frame exchange NMR spectroscopy under supercooled conditions, Biochem. Biophys. Res. Commun. 215 (2) (1995) 504–510.

[37] M. Karplus, Contact electron-spin coupling of nuclear magnetic moments, J. Chem. Phys. 30 (1959) 11–15.

[38] A. Parfondry, N. Cyr, A.S. Perlin, ^{13}C-^{1}H inter-residue coupling in disaccharides, and the orientations of glycosidic bonds, Carbohyd. Res. 59 (1977) 299–309.

[39] G.J. Batta, K.E. Kövér, J. Gervay, M. Hornyák, G.M. Roberts, Temperature dependence of molecular conformation, dynamics, and chemical shift anisotrophy of α,α-trehalose in D_2O by NMR relaxation, J. Am. Chem. Soc. 119 (1997) 1336–1345.

[40] J. Pitera, P.A. Kollman, Graphical visualization of mean hydration from molecular dynamics simulations, J. Mol. Graph. Model. 15 (1997) 355–358.

[41] C.L. Brooks, M. Karplus, B.M. Pettitt, Proteins: A Theoretical Perspective of Dynamics, Structure and Thermodynamics, Wiley-Interscience, New York, 1988.

[42] A.T. Allen, R.M. Wood, M.P. Macdonald, Molecular association in the sucrose–water system, Sugar Technol. Rev. 2 (1974) 165–180.

[43] M.-O. Portmann, G. Birch, Sweet taste and solution properties of α,α-trehalose, J. Sci. Food Agric. 69 (1995) 275–281.

[44] H. Kawai, M. Sakurai, Y. Inoue, R. Chûjô, S. Kobayashi, Hydration of oligosaccharides: anomalous hydration ability of trehalose, Cryobiology 29 (1992) 599–606.

[45] J.W. Brady, Q. Liu, Anisotropic solvent structuring in aqueous sugar solutions, J. Am. Chem. Soc. 118 (1996) 12276–12286.

[46] C.A. Andersson, S.B. Engelsen, The mean hydration of carbohydrates as studied by normalized two-dimensional radial pair distributions, J. Mol. Graph. Model. 17 (1999) 101–105.

[47] S.B. Engelsen, Molecular dynamics simulations of carbohydrate–water interactions. In Water in Biomaterials Surface Science (Ed. Marco Morra), 2001, pp. 53–89.

[48] F. Casset, T. Hamelryck, R. Loris et al., NMR, molecular modeling, and crystallographic studies of lentil lectin–sucrose interaction, J. Biol. Chem. 270 (43) (1995) 25619–25628.

[49] M. Rampp, C. Buttersack, H.-D. Lüdemann, c,T-dependence of the viscosity and the self-diffusion coefficients in some aqueous carbohydrate solutions, Carbohyd. Res. 328 (4) (2000) 561–572.

[50] I.P. Gerothanassis, Multinuclear and multidimensional NMR methodology for studying individual water molecules bound to peptides and proteins in solution: principles and applications, Progr. NMR Spectrosc. 26 (1994) 171–237.

[51] M. Billeter, Hydration water molecules seen by NMR and by X-ray crystallography, Progr. NMR Spectrosc. 27 (1995) 635–645.

[52] G. Otting, E. Liepinsh, K. Wuthrich, Protein hydration in aqueous solution, Science 254 (5034) (1991) 974–980.

[53] I. Ivarsson, C. Sandström, A. Sandström, L. Kenne, ^{1}H NMR chemical shifts of hydroxy protons in conformational analysis of disaccharides in aqueous solution, J. Chem. Soc. Perkin Trans. 2 (10) (2000) 2147–2152.

[54] P. Dais, Carbon-13 nuclear magnetic relaxation and motional behavior of carbohydrates in solution, Adv. Carbohydr. Chem. Biochem. 51 (1995) 63–131.

[55] P. Stilbs, Fourier transform pulsed-gradient spin-echo studies of molecular diffusion, Progr. NMR Spectrosc. 19 (1987) 1–45.

[56] M.M. Tirado, J.G. de la Torre, Translational friction coefficients of rigid, symmetric top macromolecules. Application to circular cylinders, J. Chem. Phys. 71 (1979) 2581–2586.

[57] J.G. de la Torre, V.A. Bloomfield, Hydrodynamic properties of complex, rigid, biological macromolecules: theory and applications, Q. Rev. Biophys. 14 (1981) 81–139.

[58] M.M. Tirado, C.L. Martinez, J.C. de la Torre, Comparison of theories for the translational and rotational diffusion coefficients of rod-like macromolecules. Application to short DNA fragments, J. Chem. Phys. 81 (1984) 2523–2526.

[59] A.J. Easteal, Tracer diffusion of water in organic liquids, J. Chem. Eng. Data 41 (4) (1996) 741–744.

[60] R.T. Boeré, R.G. Kidd, Rotational correlation times in nuclear magnetic resonance, Annu. Rep. NMR Spectrosc. 13 (1982) 319–385.

[61] C. Monteiro, C. Hervé du Penhoat, Translational diffusion of dilute aqueous solutions of sugars as probed by NMR and hydrodynamic theory, J. Phys. Chem. (2001) (in press).

[62] A.C. English, M. Dole, Diffusion of sucrose in supersaturated solutions, J. Am. Chem. Soc. 72 (1950) 3261–3267.

[63] J.K. Gladden, M. Dole, Diffusion in supersaturated solutions. II. Glucose solutions, J. Am. Chem. Soc. 75 (1952) 3900–3904.

[64] J.M. Creeth, Studies of free diffusion in liquids with the Rayleigh method, I. The determination of differential diffusion coefficients in concentration-dependent systems of two components, J. Am. Chem. Soc. 77 (1955) 6428–6440.

[65] D. Schliephake, Diffusion of sucrose in aqueous solutions, Zucker 6 (1965) 138–142.

[66] H. Uedaira, H. Uedaira, Diffusion coefficients of xylose and maltose in aqueous solution, Bull. Chem. Soc. Jpn. 42 (1969) 2140–2142.

[67] H. Uedaira, H. Uedaira, Translational frictional coefficients of molecules in aqueous solution, J. Phys. Chem. 74 (1970) 2211–2214.

[68] H. Uedaira, H. Uedaira, Sugar–water interaction from diffusion measurements, J. Sol. Chem. 14 (1) (1985) 27–34.

[69] C.S. Johnson, Diffusion ordered nuclear magnetic resonance spectroscopy: principles and applications, Progr. NMR Spectrosc. 34 (3/4) (1999) 203–256.

[70] P.J. Hajduk, E.T. Olejniczak, S.W. Fesik, One-dimensional relaxation- and diffusion-edited NMR methods for screening compounds that bind to macromolecules, J. Am. Chem. Soc. 119 (50) (1997) 12257–12261.
[71] A.R. Waldeck, P.W. Kuchel, A.J. Lennon, B.E. Chapman, NMR diffusion measurements to characterise membrane transport and solute binding, Progr. NMR Spectrosc. 30 (1997) 39–68.
[72] A. Chen, M.J. Shapiro, NOE pumping: a novel NMR technique for identification of compounds with binding affinity to macromolecules, J. Am. Chem. Soc. 120 (39) (1998) 10258–10259.
[73] S. Augé, B. Amblard-Blondel, M.A. Delsuc, Investigation of the diffusion measurement using PFG and test of robustness against experimental conditions and parameters, J. Chim. Phys. Phys.-Chim. Biol. 96 (9/10) (1999) 1559–1565.
[74] M.D. Diaz, S. Berger, Studies of the complexation of sugars by diffusion-ordered NMR spectroscopy, Carbohyd. Res. 329 (1) (2000) 1–5.
[75] L.D. Hall, S.D. Luck, Measurement of self-diffusion coefficients of carbohydrate molecules in solution using an unmodified high resolution n.m.r. spectrometer, Carbohyd. Res. 134 (1984) C1–C3.
[76] G. Widmalm, R.M. Venable, Molecular dynamics simulation and NMR study of a blood group H trisaccharide, Biopolymers 34 (8) (1994) 1079–1088.
[77] B. Hamelin, L. Jullien, C. Derouet, C. Hervé du Penhoat, P. Berthault, Self-assembly of a molecular capsule driven by electrostatic interaction in aqueous solution, J. Am. Chem. Soc. 120 (33) (1998) 8838–8847.
[78] T. Rundlöf, R.M. Venable, R.W. Pastor, J. Kowalewski, G. Widmalm, Distinguishing anisotropy and flexibility of the pentasaccharide LNF-1 in solution by carbon-13 NMR relaxation and hydrodynamic modeling, J. Am. Chem. Soc. 121 (50) (1991) 11847–11854.
[79] P. Petrova, C. Monteiro, J. Koca, C. Hervé du Penhoat, A. Imberty, Conformational behavior of nucleotide-sugar in solution: molecular dynamics and NMR study of solvated UDP-glucose in the presence of monovalent cations, Biopolymers 58 (2001) 617–635.
[80] H. Desvaux, P. Berthault, Study of dynamic processes in liquids using off-resonance rf irradiation, Progr. NMR Spectrosc. 35 (4) (1999) 295–340.
[81] G. Lipari, A. Szabo, Model-free approach to the interpretation of nuclear magnetic resonance relaxation in macromolecules. 1. Theory and range of validity, J. Am. Chem. Soc. 104 (1982) 4546–4559.
[82] G.M. Clore, A. Szabo, A. Bax, L.E. Kay, P.C. Driscoll, A.M. Gronenborn, Deviations from the simple 2-parameter model-free approach to the interpretation of N-15 nuclear magnetic-relaxation of proteins, J. Am. Chem. Soc. 112 (12) (1990) 4989–4991.
[83] D.C. McCain, J.L. Markley, Rotational spectral density functions for aqueous sucrose: experimental determinations using ^{13}C NMR, J. Am. Chem. Soc. 108 (1986) 4259–4264.
[84] J. Tropp, Dipolar relaxation and nuclear Overhauser effects in nonrigid molecules: the effect of fluctuating internuclear distances, J. Chem. Phys. 72 (11) (1980) 6035–6043.
[85] R. Brüschweiler, B. Roux, M. Blackledge, C. Griesinger, M. Karplus, R.R. Ernest, Influence of rapid intramolecular motion on nmr cross-relaxation rates. A molecular dynamics study of antamanide in solution, J. Am. Chem. Soc. 114 (7) (1992) 2289–2302.
[86] J.E. Tanner, Use of the stimulated echo in NMR diffusion studies, J. Chem. Phys. 52 (1970) 2523–2526.
[87] N. Matsunga, A. Nagashima, Transport of liquid and gaseous D_2O over a wide range of temperature and pressure, J. Phys. Chem. Ref. Data 12 (1983) 933–966.
[88] B. Leroux, H. Bizot, J.W. Brady, V. Tran, Water structuring around complex solutes: theoretical modeling of α-D-glucopyranose, Chem. Phys. 216 (1997) 349–363.